Photoacoustics 31 (2023) 100499

Contents lists available at ScienceDirect

Photoacoustics

journal homepage: www.elsevier.com/locate/pacs

Testicular torsion diagnosis and injury assessment using photoacoustic oxygenation imaging

Qianru Yang [a,1], Lulu Yang [a,1], Chihan Peng [a], Xiaoxia Zhu [a], Zhenru Wu [b], Lin Huang [c,*], Yan Luo [a,*]

[a] Department of Ultrasound, West China Hospital/West China School of Medicine, Sichuan University, Chengdu 610041, People's Republic of China
[b] Institute of Clinical Pathology, Key Laboratory of Transplant Engineering and Immunology, NHC, West China Hospital, Sichuan University, Chengdu 610041, People's Republic of China
[c] School of Electronic Science and Engineering, University of Electronic Science and Technology of China, Chengdu 611731, People's Republic of China

ARTICLE INFO

Keywords:
Photoacoustic imaging
Testicular torsion
Oxygen saturation

ABSTRACT

Testicular torsion (TT) is a medical emergency that requires immediate diagnostic evaluation. Photoacoustic imaging (PAI) has the potential to provide spatially resolved oxygen saturation (sO_2), which can serve as a valuable marker in TT diagnosis. We investigated the potential of PAI as an alternative method for TT diagnosis and testicular injury assessment. We measured sO_2 levels in different degrees of TT models using PAI at various time points. Based on histopathological results, we found that the averaged sO_2 per pixel ($\overline{sO_2}$) and reduction of $\overline{sO_2}$ (rsO_2) in twisted testicles had significant correlations with hypoxic conditions. Both $\overline{sO_2}$ and rsO_2 exhibited excellent diagnostic abilities in detecting TT and identifying ischemia/hypoxia injury following TT. Furthermore, PAI-measured sO_2 demonstrated favorable diagnostic capabilities in discriminating if the testicle had suffered irreversible injury. In summary, PAI presents a potentially promising novel approach in evaluating TT and warrants further clinical investigation.

1. Introduction

Testicular torsion (TT) is a common urological emergency in children, where the blood flow to the testicles is obstructed due to the twisting of the spermatic cord. It is estimated that TT occurs in approximately 1 in 4000 males under the age of 25 annually, accounting for 25–35% of acute scrotum cases in children [1–3].

In clinical practice, the decisions to perform detorsion or orchidectomy depends on the degree of ischemia and necrosis. Studies have shown that salvaging the testicle is unlikely in most cases when torsion lasts for more than 6 h, making orchiectomy the recommended option [4]. However, in addition to the duration of torsion, the degree of rotation is another factor associated with testicular ischemia and clinical outcomes [3,5–8]. Therefore, timely detection of TT and precise assessment of testicular viability within the recommended 24-hour treatment window are crucial in guiding prompt clinical intervention and selecting appropriate treatment modalities.

Ultrasonography (US) is currently the preferred imaging modality for evaluating TT in clinical emergencies. The presence of the whirlpool sign and absence of blood flow on Colour Doppler flow imaging (CDFI) or grey-scale US are highly indicative of TT, as extensively documented [9,10]. However, conventional US has inherent limitations, heavily relying on the expertise of sonographers and sensitivity of devices, especially in the pediatric population with small testes characterized by low vascular density and slow blood flow velocity [11,12]. Additionally, in cases of partial torsion, the preservation of blood perfusion in the testes may lead to misdiagnosis and elevate the likelihood of false negatives [13–16]. Contrast-enhanced ultrasound (CEUS) has emerged as the gold standard for diagnosing TT in recent years [17,18]. However, the high cost of US contrast agents, requirement of intravenous injection, and safety concerns associated with their use in pediatric patients have restricted the application of CEUS in emergency settings [19,20].

Photoacoustic imaging (PAI) is a rapidly developing biomedical imaging technique that is based on the photoacoustic (PA) effect. This non-invasive hybrid technique combines the high contrast of optical imaging with the high spatial resolution of ultrasound imaging to

* Corresponding authors.
E-mail addresses: lhuang@uestc.edu.cn (L. Huang), yanluo@scu.edu.cn (Y. Luo).
[1] Co-first author

https://doi.org/10.1016/j.pacs.2023.100499
Received 16 December 2022; Received in revised form 19 April 2023; Accepted 24 April 2023
Available online 25 April 2023

reconstruct structural or functional images of tissues from captured ultrasound signals, known as photoacoustic signals (PAS). These signals are evoked from endogenous chromophores, such as hemoglobin, melanin, and lipids, which are excited by pulsed laser light [21–23]. Hemoglobin is the predominant substance responsible for strong optical absorption in blood vessels within the range of light wavelengths from 690 to 850 nm. By analyzing the distinct optical absorption peaks of oxygenated hemoglobin (HbO_2) and deoxygenated hemoglobin (HbR), for example, at 840 nm and 760 nm, respectively [24,25], PAI demonstrates the potential to accurately quantify levels of oxygenation and provide spatially resolved measurements of oxygen saturation (sO_2). This technique is label-free and non-invasive because the laser fluence falls within the safety range [26]. Studies have developed PAI measurements of sO_2 for evaluating tumor microenvironments, characterizing renal function, assessing myocardial ischemia, and examining ischemia-reperfusion in fingers [27–30]. In these studies, HbO_2 and HbR have proven to be valuable markers for differentiating between normal and pathological tissues [31,32].

TT can result in ischemia, hypoxia, and ultimately necrosis. The hypoxia stimulation may lead to an increase in the expression of hypoxia-inducible factor 1-alpha (HIF-1α) and a decrease in tissue sO_2 levels [33,34]. In theory, sO_2 measurements obtained through PAI could potentially serve as a diagnostic tool for TT and detect changes in hemoglobin redox states during clinical emergencies. However, there have been no studies to date that have investigated the usefulness of PAI in evaluating TT.

The main aim of this study is to investigate the feasibility of using PAI to detect TT early and estimate the degree of testicular injury following TT, based on histopathological changes.

2. Methods

2.1. Animals

A total of 50 male New Zealand rabbits weighing between 2.2 and 3.0 kg were provided and housed under standard living conditions for a 2-week acclimatization period. All animal experiments were conducted in compliance with the National Institutes of Health Guide for the Care and Use of Laboratory Animals and were approved by the Animal Care and Use Committee of West China Hospital (License Number: 20220519012).

2.2. TT modeling

Surgery was performed on rabbits after they were anesthetized with Zoletil at a dosage of 5 mg/kg intramuscularly, followed by intraperitoneal administration of 1% pentobarbital sodium at a dosage of 3 ml/kg. Prior to the surgery, the inguinal and scrotal regions were shaved and sterilized under aseptic conditions. Incisions were made at a distance of 1–2 cm above the scrotum, while maintaining sterile conditions. The spermatic cord was rotated in a counter-clockwise direction and subsequently affixed to the muscular wall at the same level. The animals were subjected to torsion at 0° (sham operation, group S; n = 5), 180° (group A; n = 15), 360° (group B; n = 15), and 720° (group C; n = 15) in a randomized manner. For the torsion groups (group A, B, C), rabbits were further divided into three subgroups (n = 5 for each subgroup) based on the time of sacrifice after the operation (2 h, 4 h, 6 h). Postoperative analgesia was administered intramuscularly with 0.2 ml/kg of meloxicam.

2.3. Colour Doppler ultrasound evaluation

Ultrasound examinations were performed before and after the operation using an M9cv ultrasound system (Mindray Medical Solutions, Shenzhen, China) equipped with a L12–4 s transducer (4–12 MHz). Dynamic imaging of color Doppler was obtained in a longitudinal section for at least 30 s under high rate flow mode. The intratesticular blood flow of the testicle was graded on a scale of 0–4 by a sonographer with over 8 years of experience in clinical US diagnosis, based on the criteria established by Coley et al. [35]. This evaluation was conducted without knowledge of the pathological results.

2.4. Photoacoustic imaging system and data acquisition

As illustrated in Fig. 1, to collect the PA signal, we used a 128-element concave ultrasound transducer array (Japan Probe Corporation, Yokohama, Japan) as described in our previous research [36–38]. The array was connected to homemade pre-amplifiers with a gain of 56 dB and eight DAQ modules (5105, NI). The transducer had a central frequency of 5.0 MHz and a radius of 50 mm. We employed a Q-switched Nd:YAG pumped optical parametric oscillator system (Surelite, Continuum, California) for illumination in the range of 700–960 nm. The pulse duration was approximately 4 ns at a repetition rate of 20 Hz. The excitation laser was transmitted to the tissue through an optic fiber bundle, providing line-shaped illumination with dimensions of 40 mm (long axis) × 10 mm (short axis).

The optical fluence incident on the tissue surface was estimated to be 5 mJ/cm^2, which is below the maximum permissible exposure limit recommended by the American National Standards Institute [26]. To account for fluctuations in the laser output, 5% of the light energy was directed through a beam splitter to a laser energy meter (Pulsar-1, Ophir, Jerusalem, Israel).

During the experiment, the PA signals captured by the transducer underwent amplification through a pre-amplifier consisting of 64 channels with a bandwidth ranging from 0.2 to 10 MHz and a gain of 56 dB. The signals were then subjected to a 2:1 multiplexing and averaged ten times under a laser working frequency of 10 Hz or less. Subsequently, the signals were transferred to a 64-channel analog-to-digital system comprising eight PXIe5105 cards (National Instrument, Texas, USA). The PAI system was controlled by an onboard computer (PXIe8840, National Instrument, Texas, USA) which also functioned as a device for signal storage. Each PAI image was acquired within approximately 1 s. The PA image reconstruction was performed using a delay-and-sum algorithm in Matlab (R2016b, Mathworks, Inc., MA, USA), as previously mentioned [39].

The PAI was assessed before and at 2, 4, and 6 h after TT surgery. The animals were placed in a supine position on an oblique panel in a sink, with the water temperature maintained at around 35 ℃. The PAI probe was positioned longitudinally directly above the testicle and illuminated vertically. The PA scanning was performed in the largest longitudinal section, and signals were consistently acquired at wavelengths of 760 nm and 840 nm, with an acquisition rate of 1 frame per second. The data were averaged over time for 10 consecutive frames.

2.5. Image reconstruction and analysis

All data were reconstructed in real-time using the back-projection algorithm in Labview (NI, USA) and stored for subsequent processing by Matlab. To eliminate noise, a 0.2–10 MHz filter was applied during offline processing. Additionally, a laser energy meter (Pulsar-1, Ophir, Jerusalem, Israel) was used to eliminate the impact of optical fluence variation at the two wavelengths (840 nm and 760 nm) on sO_2 calculation, as shown in Fig. 1.

In this study, it was assumed that HbR and HbO_2 are the primary absorbers.

Then, the generated PA signal intensity ($P(\vec{r},\lambda)$) can be described as follows:

$$P(\vec{r},\lambda) = \Gamma\mu_a(\vec{r},\lambda)\Phi(\vec{r},\lambda)$$

Where Γ is known as the Grueneisen coefficient, $\mu_a(\vec{r},\lambda)$ and $\Phi(\vec{r},\lambda)$ are the optical absorption coefficient and optical fluence, respectively. In

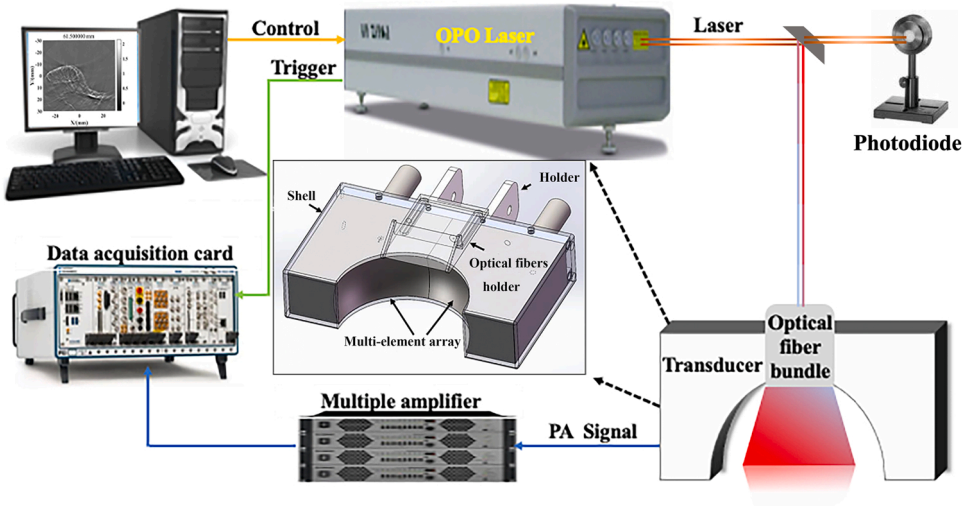

Fig. 1. Schematic of the PA imaging system.

addition, based on the dual-wavelength acquisitions at 840 nm and 760 nm, the PA data were unmixed to get the concentrations of HbR and HbO_2 according to the Eq. [40].

$$\mu_a(\vec{r},\lambda) = \varepsilon_{HbR}(\lambda)[HbR](\vec{r}) + \varepsilon_{HbO_2}(\lambda)[HbO_2](\vec{r})$$

Where ε (λ) represents the known molar extinction coefficient of HbR or HbO_2 at wavelength λ.

The sO_2 mapping calculation in the testis was performed using the formula $sO_2 = [HbO_2]/([HbO_2] + [HbR])$. The imaging of sO_2 distribution allowed for the selection of the region of interest (ROI), which was limited to the 2 mm diameter area located directly beneath the testicular membrane. The average sO_2 per pixel ($\overline{sO_2}$) was then obtained from the selected ROI (Fig. 2). Three distinct ROIs were identified, and the mean $\overline{sO_2}$ was subsequently calculated as the final outcome.

2.6. Histopathological assessment

The twisted testes were surgically removed at specific time intervals. The excised tissues underwent histological examination using hematoxylin and eosin (H&E) staining and immunohistochemical (IHC) staining with HIF-1α. Microscopic images of the stained tissues were captured at magnifications of 200 × and 400 × using a light microscope.

Based on the histopathological changes, the twisted testicle was evaluated using Cosentino's histological grading criteria [41,42]. It was classified as normal (grade 1), ischemia/hypoxia injury (grade 2 or above), or severe injury/necrosis (grade 3 and grade 4). The degree of HIF-1α expression, which indicates the presence of hypoxic conditions, was assessed for each histological section using a scoring system ranging from 1 to 3. The scoring was based on both the expression rate and staining intensity. Cases with no or mild staining and an expression rate below 30% were assigned a score of 1, while those with moderate staining and an expression rate ranging from 30% to 70% were given a

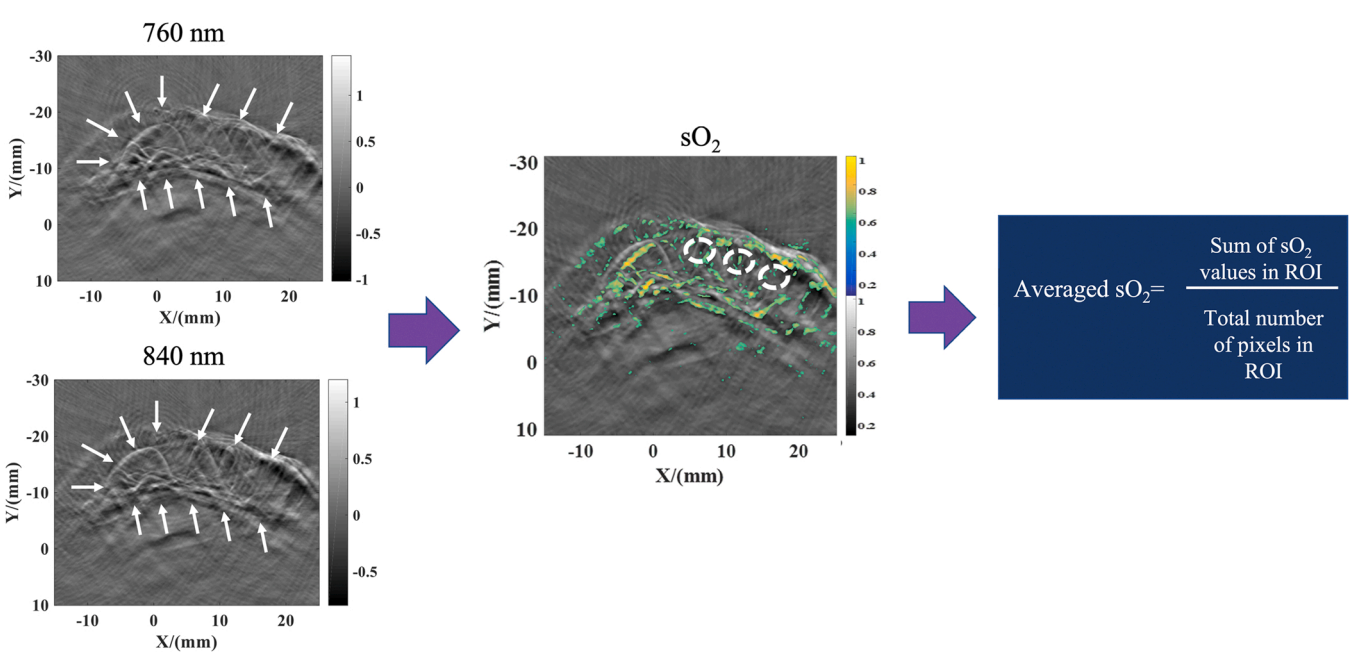

Fig. 2. The calculation of the average oxygen saturation (sO_2) was based on the dual-wavelength PA imaging at 840 nm and 760 nm. The white arrows were used to indicate the border of the testicles, while the white circles denoted the regions of interest (ROI).

score of 2. Finally, cases with intense staining and an expression rate above 70% were scored as 3.

2.7. Statistical analysis

The Shapiro–Wilk test was utilized to analyze the data distribution. One-way ANOVA with Tukey's post hoc test was used to compare PAI measurements of sO_2 among different groups at various time points for normally distributed data, while non-normally distributed data was analyzed using the nonparametric Kruskal-Wallis test. Spearman's rank coefficients were calculated to evaluate the associations between CDFI score or sO_2 and pathological hypoxic conditions (HIF-1α expressions). The diagnostic performance of the CDFI score and sO_2 in TT diagnosis, specifically in identifying pathological ischemia/hypoxia injury or severe injury/necrosis, was assessed by calculating the areas under the receiver operating characteristic (ROC) curves (AUCs) with 95% confidence intervals (CIs). The sensitivity and specificity were determined using the optimal cutoff points that maximized the Youden index. SPSS (version 26.0, SPSS, Chicago, IL, United States), GraphPad software (version 7.00; GraphPad Software, San Diego, CA, USA), or MedCalc (version 10.4, MedCalc Software, Mariakerke, Belgium) were used for statistical analyses and graphs. Differences were considered significant when P values were < 0.05.

3. Results

3.1. The PA and CDFI imaging of testicles

The figures in Fig. 3 depict the pre- and postoperative PA and CDFI images of the testicles. As the degree of torsion increased, the CDFI signals were scarcely observed in groups B and C. The PA imaging displayed the borders of the testicles and the boundary between the scrotal skin and testicular parenchyma. However, no significant correlations were found between the PA signals in the testicular parenchyma and the degree of torsion.

3.2. The changes of sO_2 obtained by PAI

Two hours after torsion, the $\overline{sO_2}$ of the testes in groups B and C were significantly lower than those in group S. However, no statistically significant difference was observed between groups A and S. At 4 and 6 h postoperatively, the $\overline{sO_2}$ levels of the testes in the TT groups (groups A, B, and C) were significantly decreased compared to those in group S. However, no significant differences in $\overline{sO_2}$ levels were detected between the torsion groups at each time point. For each torsion group, the PAI-measured $\overline{sO_2}$ after surgery was found to be significantly decreased when compared to the preoperative values (as shown in Fig. 4 and Table 1). There were no significant differences in $\overline{sO_2}$ at different postoperative time points.

The reduction of $\overline{sO_2}$ (rsO_2) at each time point was determined by comparing it to the preoperative level (Fig. 5). At the 2-hour postoperative mark, both groups B and C exhibited significantly higher rsO_2 values than group S, with measurements of (10.41 ± 1.22)% and (15.05 ± 2.13)%, respectively. Notably, the rsO_2 levels across the experimental groups increased with the duration of torsion time. Until 6 h postoperation, the rsO_2 values in groups B and C reached (20.69 ± 2.01)% and (23.79 ± 6.40)%, respectively. However, no statistically significant differences in rsO_2 were observed among the postoperative time points for the same degree of torsion group.

3.3. Histopathology changes

The testicles in group S exhibited normal seminiferous tubules with spermatogenic cells and mature spermatozoa arranged in an orderly manner (Fig. 6a). Out of the 45 animals subjected to experimentation, 80% (36) of the testes showed ischemia/hypoxia injury. The histopathological examination of these testicles revealed varying degrees of interstitial hemorrhage and a reduction in the spermatogenic epithelium (Fig. 6b-d). Additionally, 40% (18) of the testicles experienced severe injury/necrosis, which was evidenced by irreversible changes such as the destruction of bounded seminiferous tubules, sloughed cells in the lumen, and nucleus pyknosis (refer to Fig. 6c, d).

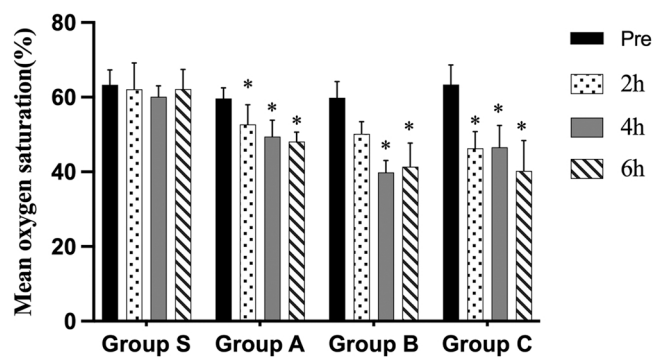

Fig. 4. The changes in mean oxygen saturation were documented by PAI in torsion testes in groups S, A, B, and C. (*: $P < 0.05$ vs. Pre).

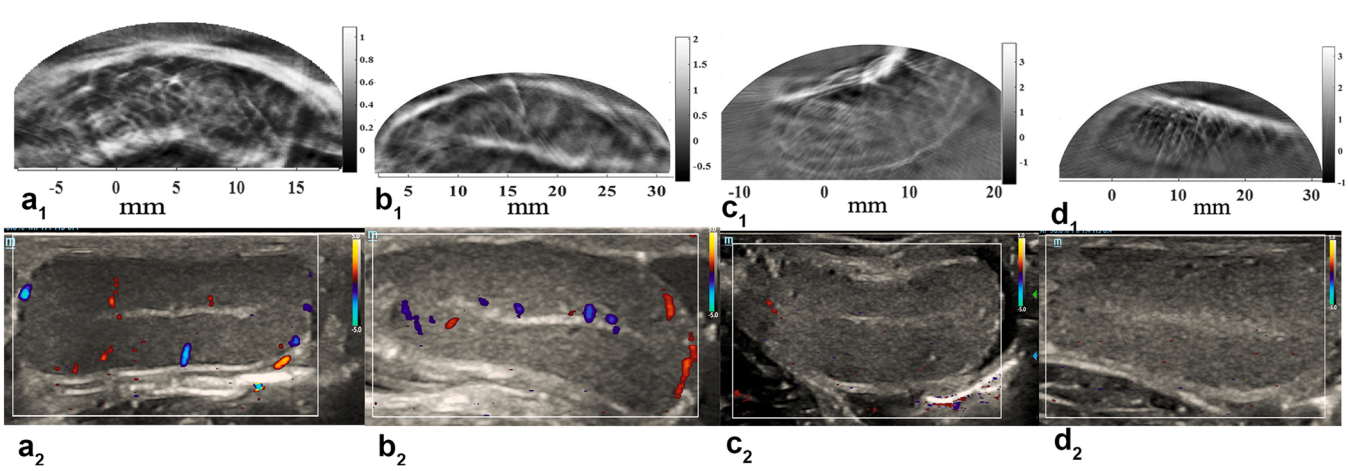

Fig. 3. The PA imaging at a wavelength of 760 nm (upper, a_1–d_1) and CDFI imaging (down, a_2–d_2) of testicles in each group at 6 h after operation. (a) group S, (b) group A, (c) group B, and (d) group C.

Table 1
The mean oxygen saturation ($\overline{sO_2}$) in different degrees of testicular torsion at different time points (%).

Groups	Pre	2 h	4 h	6 h
S	63.29 ± 4.00	62.10 ± 7.07	60.08 ± 2.95	62.16 ± 5.27
A	59.63 ± 2.87	52.69 ± 5.30^{p}	49.43 ± 4.43^{s,p}	48.11 ± 2.53^{s,p}
B	59.85 ± 4.32	50.15 ± 3.31^{s}	39.84 ± 3.16^{s,a,p}	41.35 ± 6.34^{s,p}
C	63.39 ± 5.23	46.31 ± 4.43^{s,p}	46.59 ± 5.83^{s,p}	40.21 ± 8.15^{s,p}

s: P < 0.05 vs. group S; a: P < 0.05 vs. group A;
p: P < 0.05 vs. Pre

3.4. Expression of HIF-1α and its correlation with sO_2 obtained by PAI

HIF-1α was scarcely expressed in normal testicular tissue. However, following TT, the expression of HIF-1α increased in both spermatogenic cells and Leydig cells across all experimental groups, as depicted in Fig. 7. Nonetheless, no statistically significant differences were observed in HIF-1α expression among the groups at 2 h post-operation. At 6 h after the operation, HIF-1α expression was significantly higher in groups B and C than in the control group (both P < 0.05), as shown in Fig. 8. In group C, the expression levels of HIF-1α were significantly elevated at 4 and 6 h post-operation compared to pre-operation (P = 0.008 and P = 0.046, respectively).

At 6 h after the surgery, a negative correlation was observed between the $\overline{sO_2}$ and HIF-1α expression. The Spearman correlation coefficient was − 0.66 (P = 0.002). Furthermore, a significant positive correlation was found between the expression of HIF-1α and rsO_2, with a correlation coefficient of 0.70 (P = 0.001). However, there was no significant correlation between the CDFI score and HIF-1α expression (P = 0.07).

3.5. The diagnostic performance of PAI in early detecting TT

When using the operation as the benchmark, the measurement of sO_2 by the PA demonstrated exceptional diagnostic capability in detecting TT, as shown by the AUCs of 0.93 (95% CI, 0.82–1.00) for both $\overline{sO_2}$ and rsO_2 (Fig. 9a). Table 2 presents the optimal cutoff values for $\overline{sO_2}$ and rsO_2, as determined by the Youden index. Referring to these cutoff values, the sensitivity and specificity of $\overline{sO_2}$ or rsO_2 in the diagnosis of TT were both found to exceed 80%. In contrast, for CDFI, the AUC of scores for diagnosing TT was 0.82 (95% CI, 0.72–0.93), with a sensitivity of 100% and a specificity of 73%.

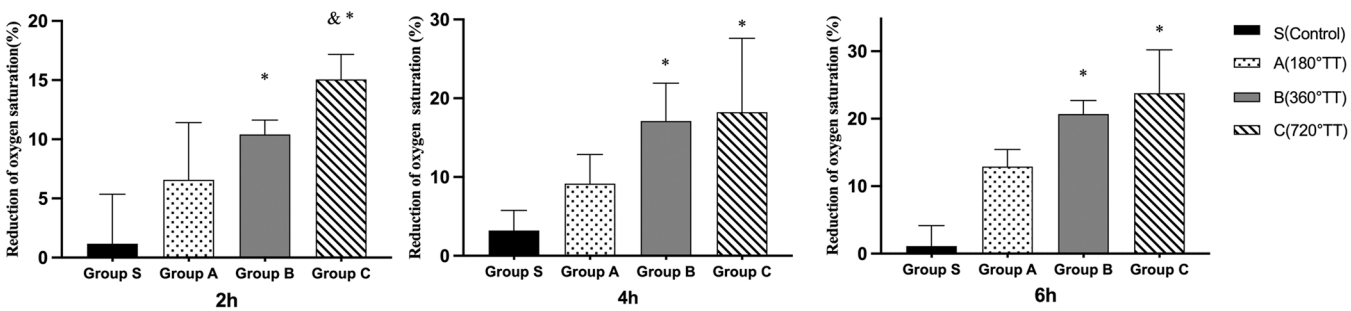

Fig. 5. The reduction of oxygen saturation (rsO_2) was documented by PAI at each time point after operation in different groups. (*: P < 0.05 vs. Group S; &: P < 0.05 vs. Group A).

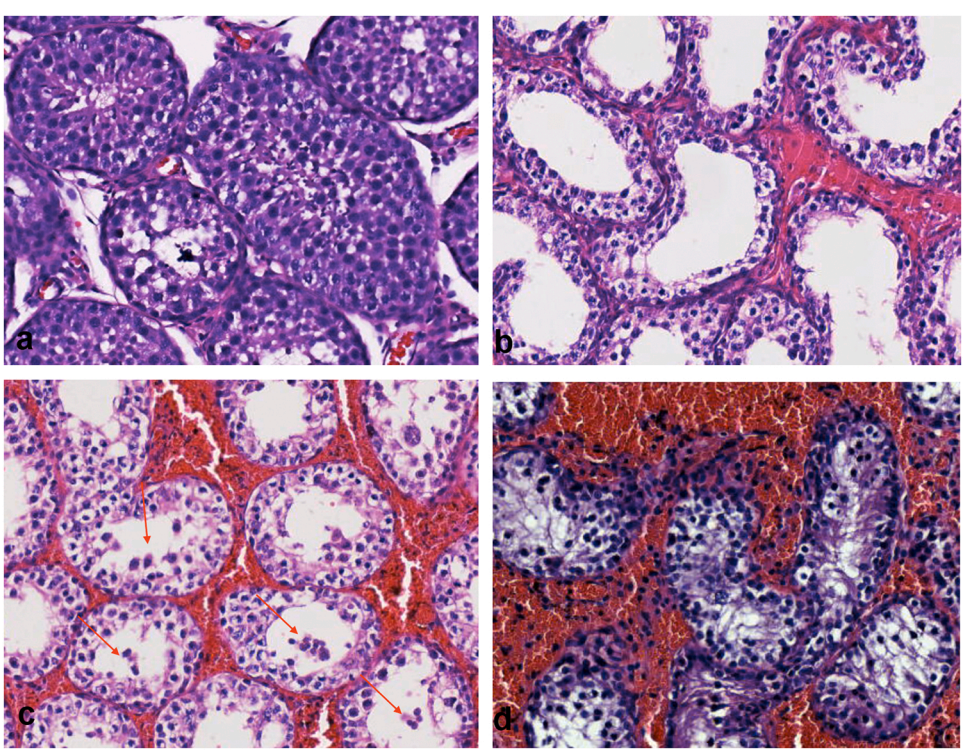

Fig. 6. Histologic findings of testicles in group S and torsion groups. (a) Testicles in group S. (b) At 4 h post-operation, minor injury with diminished spermatogenic epithelium and mild interstitial hemorrhage were observed in 180° testicular torsion. (c) After 6 h following operation, severe injury with disordered sloughed cells in the lumen (red arrows) and aggravated interstitial hemorrhage were demonstrated in 360° testicular torsion. (d) Necrosis was presented in 720° testicular torsion after 6 h with destructed bounded seminiferous tubules and extensive interstitial hemorrhage. (All images were taken at an original magnification of ×200.).

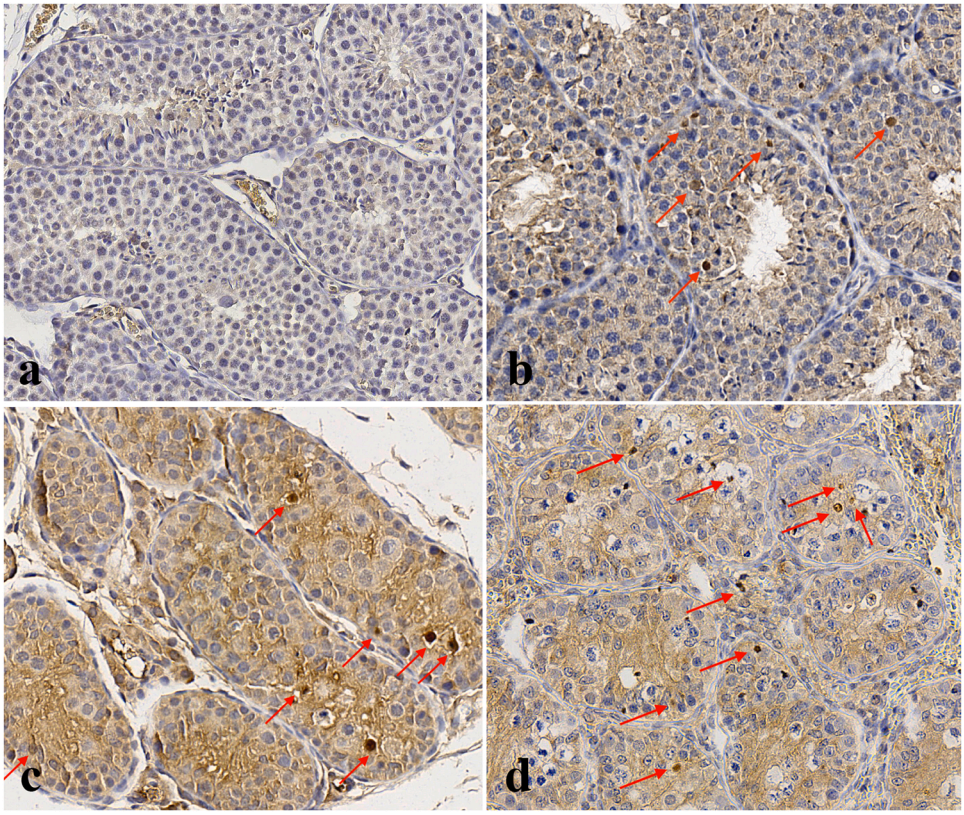

Fig. 7. Expression of HIF-1α by immunohistochemistry: (a) There was no significant expression of HIF-1α in normal testicular tissue. (b) The cytoplasm showed moderate staining, and a few positive nuclei were observed in 180°testicular torsion 2 h after the operation. (c) The cytoplasm displayed strong staining, and the number of positive nuclei increased in 360°testicular torsion 2 h after the operation. (d) More spermatogenic cells and Leyding cells with positive nuclei were observed at 4 h after the operation following 720°testicular torsion. (Red arrow: positive nucleus) (Original magnifications ×200).

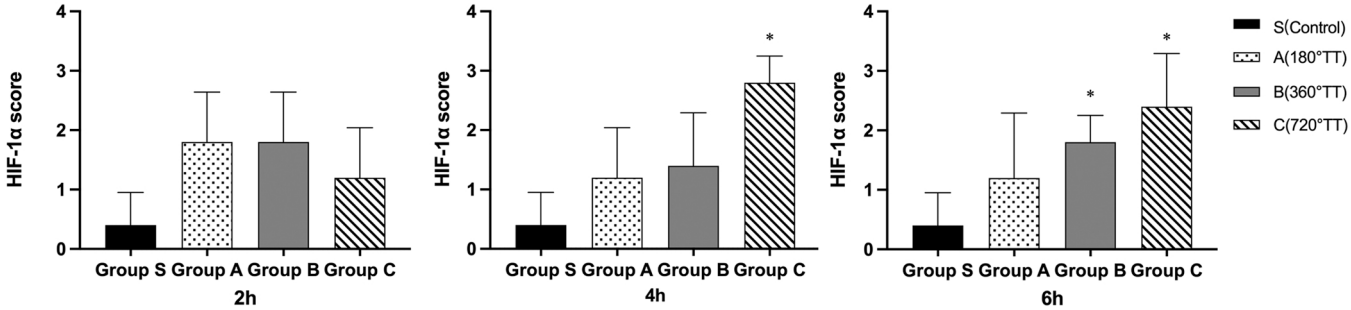

Fig. 8. The scores of HIF-1α expression in each group at various times after testicular torsion. (*: $P < 0.05$ vs. Group S).

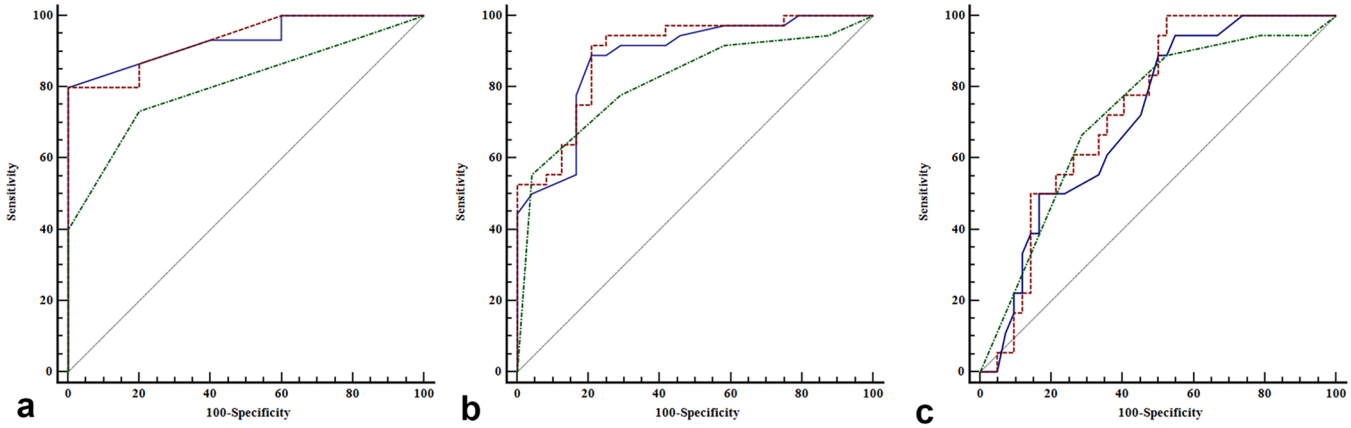

Fig. 9. The receiver operating characteristic (ROC) curves of $\overline{sO_2}$ (represented by blue lines), rsO_2 (represented by red dot lines), and CDFI score (represented by green dot lines) were analyzed for their effectiveness in diagnosing testicular torsion (a), identifying testicular ischemia/hypoxia injury (b), and severe injury/necrosis (c).

Table 2
The diagnostic capability of oxygen saturation (sO_2) obtained by PAI in detecting testicular torsion.

Variable	AUC (95%CI)	Cutoff value (%)	Sensitivity (%)	Specificity (%)
$\overline{sO_2}$	0.93 (0.82–1.00)	56.1	100	86.7
rsO_2	0.93 (0.82–1.00)	7.35	80	100

3.6. The diagnostic performance of PAI in identifying ischemia/ hypoxia injury after TT

Regarding the pathological changes that occur after TT, the AUCs of $\overline{sO_2}$ and rsO_2 for identifying ischemia/hypoxia injury were found to be 0.88 and 0.90, respectively. The corresponding sensitivity and specificity were both above 79%, as shown in Fig. 9b and Table 3. Additionally, the AUC of CDFI scores was determined to be 0.81 (95% CI, 0.71–0.92), with a sensitivity of 81.5% and specificity of 72.6%.

3.7. Diagnostic performance of PAI in identifying severe injury/necrosis after TT

The AUCs of $\overline{sO_2}$ and rsO_2 were both greater than 70% when distinguishing between testicles that had suffered severe injury/necrosis and those that had not (Fig. 9c, Table 4). A diagnostic specificity of 94.4% was found for $\overline{sO_2}$ using a cutoff value of 53.3%. In distinguishing severe injury/necrosis, the sensitivity was 100% when rsO_2 was above 7.82%. Comparable diagnostic performance was observed for CDFI scores in the diagnosis of severe injury/necrosis, with an AUC of 0.72 (95% CI, 0.59–0.84). The corresponding sensitivity and specificity were 64.3% and 82.1%, respectively.

4. Discussion

Timely diagnosis and appropriate treatment of TT are crucial in preventing irreversible testicular injury and ensuring testicular survival [43,44]. In clinical practice, the decisions to perform detorsion or orchidectomy depends on the duration of symptoms and the surgeon's subjective evaluation of the twisted testes after incision, without prior knowledge of the underlying pathological changes. In this study, we aimed to investigate the potential of PAI in diagnosing TT and determining the degree of testicular injury. To achieve this, we established various degrees of TT models in rabbits and used pathological changes as the gold standard for assessment.

The pathological changes that occur following TT with a rotated vascular pedicle are due to obstructed arterial inflow and venous drainage, resulting in ischemia and hypoxia. This leads to increased capillary pressure and permeability, allowing for the leakage of red blood cells through the damaged basement membrane and widened endothelial cell gap, resulting in varying degrees of interstitial hemorrhage (Fig. 6). Interestingly, in some severe torsion cases, we observed an increase in spotted PA signals. However, this phenomenon was not present in every twisted case, and the increased signals did not consistently correspond with the degree of hemorrhage. This can be attributed to the complex pathological changes that occur after TT. With prolonged duration, venous stasis can lead to microthrombus formation and eventual infarction, which may diminish the PA signal. Unlike CDFI, the PA signals captured are primarily dependent on the concentration of hemoglobin rather than the flow of blood. Thus, finding the rules governing the variations in PA signals after TT, which affects both inflow and outflow, presents a significant challenge. This is one of the reasons we chose to concentrate on dual-wavelength PA functional imaging at 840 nm and 760 nm, as opposed to vascular structural imaging at a wavelength of 534 nm, to evaluate TT.

Table 3
The diagnostic capability of oxygen saturation (sO_2) obtained by PAI in identifying the ischemia/ hypoxia injury after testicular torsion.

Variable	AUC (95%CI)	Cutoff value (%)	Sensitivity (%)	Specificity (%)
$\overline{sO_2}$	0.88 (0.79–0.97)	50.9	79.2	88.9
rsO_2	0.90 (0.81–0.98)	8.9	91.7	79.2

Table 4
The diagnostic capability of oxygen saturation (sO_2) obtained by PAI in identifying severe injury/necrosis after testicular torsion.

Variable	AUC (95%CI)	Cutoff value (%)	Sensitivity (%)	Specificity (%)
$\overline{sO_2}$	0.72 (0.59–0.85)	53.3	45.2	94.4
rsO_2	0.74 (0.62–0.87)	7.82	100	47.6

In cases of ischemia/hypoxia, the testicles are inevitably accompanied by changes in sO_2. Early and accurate detection of hypoxic conditions (sO_2) holds theoretical value in diagnosing TT and assessing injury degree. In recent years, local blood sO_2 detection has been applied in medical fields, such as evaluating tumor malignancy [45], diagnosing cerebral desaturation and vasospasm in stroke patients [46], and predicting the survival rate of plastic surgery flaps [47]. However, limited research has analyzed the significance of sO_2 in TT assessment. Currently, clinical techniques utilized for detecting sO_2 include pulse oximetry, blood oxygen level-dependent magnetic resonance (BOLD-MRI), and positron emission tomography (PET) [48,49]. Pulse oximetry is predominantly employed for monitoring peripheral blood sO_2, while BOLD-MRI and PET are costly and infrequently utilized diagnostic tools in emergency settings. Near-infrared spectroscopy (NIRS) analysis and diffuse optical tomography (DOT) also employ near-infrared wavelengths ranging from 690 nm to 850 nm to determine the sO_2 in the region of interest, similar to PAI. This is based on the differences in the infrared absorption coefficient of HbO_2 and HbR in biological tissues at different wavelengths [50,51]. However, the low spatial resolution of both NIRS and DOT presents challenges in imaging the sO_2 distribution of tissues.

PAI is a non-invasive method that quantifies oxygenation and provides spatially resolved sO_2 values for specific tissue regions. Although it is theoretically possible to compute both the total blood oxygen ($HbT = [HbO_2] + [HbR]$) and sO_2 concurrently, the heterogeneous tissue's varying light attenuation results in a greater margin of error in the HbT obtained [52]. Moreover, clinicians are more familiar with and commonly use sO_2 instead of the concentration of HbO_2 or HbR. Therefore, we selected sO_2 as the assessment parameter instead of the hemoglobin concentration. It is worth noting that the sO_2 values obtained through PAI are calculated as an average of both arterial and venous values, resulting in a final $\overline{sO_2}$ value that is the pixel-averaged sO_2 of the entire vascular bed within the ROI. In this study, we successfully demonstrated the use of PAI in measuring changes in sO_2 levels in testicular tissues after TT.

Compared to organs such as the liver and kidney, which have ample blood supply, the testicle exhibits relative hypovascularity. Using PAI, we determined the $\overline{sO_2}$ of a normal testicle to be (63.29 ± 4.00)%, which is consistent with the previously reported range of 57–61% measured by NIRS [53–56]. After TT, we observed a significant reduction in the sO_2 levels of the twisted testicle at 2 h. At this time point, group B and C exhibited rsO_2 levels of (10.41 ± 1.22)% and (15.05 ± 2.13)%, respectively, which were significantly higher than those in the control group. Furthermore, the $\overline{sO_2}$ levels in all torsion groups decreased below 50%. The rsO_2 in groups B and C were (20.69 ± 2.01)% and (23.79 ± 6.40)%, respectively. These findings suggest that PAI is sensitive to hypoxic

conditions following TT.

However, group A did not show a significant decrease in rsO_2 compared to the control group at any point during the observation period following TT. This lack of significant decrease in rsO_2 can be attributed to the mild degree of torsion, which did not result in significant injury during the observation period. This finding may also explain the clinical observation that testicles can be salvaged following TT that lasts longer than 6 h. On the other hand, there were no statistically significant variations in rsO_2 levels observed among the experimental groups during the 4-hour and 24-hour postoperative periods. This could potentially be attributed to the diminishing differences in sO_2 levels between varying degrees of torsion as the duration of the experiment progressed.

AydogduO et al. [53] used NIRS to assess changes in sO_2 levels in rats subjected to varying degrees of TT. One hour post-torsion, the authors observed decrease in testicular sO_2 levels from 59% to 41% in rats subjected to 360° TT (representing a reduction of approximately 18%), and from 61% to 36% in rats subjected to 720° TT (representing a reduction of approximately 25%). Three hours post-torsion, the testicular sO_2 levels in the 360° and 720° TT groups decreased by 25% and 30%, respectively. Hallacoglu et al. [55] conducted a study involving four adult rabbits, in which they utilized NIRS to detect changes in testicular tissue sO_2 following 540° and 720° torsion. Their findings indicated a decrease in sO_2 by (36 ± 2)% on the torsion side compared to the opposite side. In contrast to previous reports obtained through NIRS, our investigation measured lower sO_2 using PAI after TT. This discrepancy may be explained by the limitations of NIRS, which has low spatial resolution and may not accurately sample the ROI. The utilization of ROI selection with low spatial resolution over large areas may lead to a decrease in the averaged sO_2 due to unwanted background signals.

HIF-1 is a transcription factor that facilitates adaptive responses to ischemia/hypoxia. HIF-1α, a subtype of HIF-1, is known to increase under hypoxic conditions, and HIF-1α staining is commonly used to reveal pathological hypoxia [57]. Our study observed an increase in HIF-1α expression across all torsion groups, with significant elevation at 6 h post-surgery. Additionally, the sO_2 levels obtained through PAI exhibited significant correlations with the expressions of HIF-1α. These findings suggest that PAI has the potential to be a valuable tool for quantifying tissue oxygenation saturation.

In clinical settings, color Doppler US has been reported to have a sensitivity range of 69.2–100% and a specificity range of 52.9–100% in the diagnosis of TT [9,58–60]. It is important to note that the accuracy of US diagnosis depends on the operator, devices used, and characteristics of the population being investigated. Therefore, surgical exploration is strongly recommended when there is clinical suspicion of TT, especially in pediatric patients, regardless of the US examination results [61]. In this experiment, the use of PAI to measure sO_2 showed exceptional ability in the early detection of TT, with AUC values of 93%, surpassing those obtained with CDFI. The corresponding sensitivity and specificity were both above 80%. These excellent diagnostic results suggest that PAI has promising clinical potential for the diagnosis of TT, allowing for timely clinical intervention while avoiding unnecessary surgical exploration.

In situations where the degree and duration of torsion are unknown, PAI demonstrates exceptional diagnostic performance in identifying the presence of pathological ischemic/hypoxic injury in a twisted testicle. The AUCs of $\overline{sO_2}$ and rsO_2 were 88% and 90%, respectively, surpassing that of CDFI. The corresponding diagnostic sensitivity and specificity were both above 79%. In discriminating whether the testicle had suffered severe injury/necrosis, we observed good diagnostic capabilities in the $\overline{sO_2}$ and rsO_2 measured by PAI with AUCs of 0.72 and 0.74, respectively. These AUC values were comparable to those of CDFI. When $\overline{sO_2}$ decreased below 53.3%, the specificity in distinguishing irreversible necrosis increased to 94.4%. This indicates the possibility of unsalvageable TT, and therefore, orchiectomy may be recommended as the preferred treatment. Conversely, using a cutoff value of 7.82% for rsO_2, the sensitivity in identifying severe injury/necrosis reached 100%, while the specificity was only 47.6%. In this situation, the degree of injury may be overestimated. Hence, in the identification of necrosis following TT, PAI exhibits some value, though not ideal. The possible explanation is that in cases of severe injury/necrosis, infarction may occur, and the presence of necrotic tissue may impact the accurate detection of sO_2. Moreover, in certain severe cases of TT, the swollen and thickened scrotal walls, along with heightened vascularity, may augment the absorption and scattering of light. This could potentially weaken the intensity of the light signal that penetrates the testicular parenchyma, hindering detection and resulting in measurement inaccuracies. Therefore, additional research is required to examine the diagnostic potential of photoacoustic sO_2 in assessing severe injury/necrosis after TT.

Although the results presented are promising, it is important to acknowledge several limitations of this study. Firstly, there is currently no universally accepted method for measuring tissue oxygenation saturation, and further verification is necessary to determine whether the sO_2 obtained by PAI accurately reflects actual tissue sO_2. Secondly, while the PAI system utilized in this trial has a strong experimental foundation, this is the first time it has been applied to TT assessment. To achieve functional imaging of the testicles, we optimized the parameters at the expense of temporal resolution, which could potentially lead to sampling errors. Additionally, the algorithm currently employed does not account for additional optical absorption and scattering caused by the scrotal skin and other heterogeneous tissues, which may result in measurement inaccuracies due to the uncertainty of optical fluence distribution. Optical methods will be employed in the subsequent study for reference purposes, with a focus on achieving greater precision in the detection of sO_2. Finally, it is important to note that this is only a preliminary animal study, and further validation of the results is necessary in larger animals and even human volunteers.

Despite the limitations inherent in this study, it represents the first attempt to examine PAI in TT assessment. In summary, the PAI obtained oxygenation saturation at wavelengths of 760 nm and 840 nm demonstrated good diagnostic capabilities for both TT diagnosis and testicular injury assessment. These findings show significant promise for further clinical application.

Funding

This work was supported by Post-Doctor Research Project, West China Hospital, Sichuan University Grant No.2021HXBH039.

Declaration of Competing Interest

The authors declare that they have no known competing financial interests or personal relationships that could have appeared to influence the work reported in this paper.

Data Availability

Data will be made available on request.

Acknowledgments

None.

References

[1] L.C. Zhao, M.F. Romano, M.H. Katz, et al., Pediatric testicular torsion epidemiology using a national database: incidence, risk of orchiectomy and possible measures toward improving the quality of care, J. Urol. 186 (5) (2011) 2009–2013.

[2] T. Liang, P. Metcalfe, W. Sevcik, et al., Retrospective review of diagnosis and treatment in children presenting to the pediatric department with acute scrotum, Am. J. Roentgenol. 200 (5) (2013) W444–W449.
[3] J. Mansbach, P. Forbes, C. Peters, Testicular torsion and risk factors for orchiectomy, J. Adolesc. Health 2 (34) (2004) 143–144.
[4] Z. Pogorelić, K. Mustapić, M. Jukić, et al., Management of acute scrotum in children: a 25-year single center experience on 558 pediatric patients, Can. J. Urol. 23 (6) (2016), 8594-601.
[5] A.C. Dias, J.R. Alves, H. Buson, et al., The amount of spermatic cord rotation magnifies the time-related orchidectomy risk in Intravaginal testicular torsion, Int. Braz. J. Urol. 42 (6) (2016) 1210–1219.
[6] A.S. Howe, V. Vasudevan, M. Kongnyuy, et al., Degree of twisting and duration of symptoms are prognostic factors of testis salvage during episodes of testicular torsion, Transl. Androl. Urol. 6 (6) (2017) 1159.
[7] T. Yecies, J. Bandari, F. Schneck, et al., Direction of rotation in testicular torsion and identification of predictors of testicular salvage, Urology 114 (2018) 163–166.
[8] A.E. Sessions, R. Rabinowitz, W.C. Hulbert, et al., Testicular torsion: direction, degree, duration and disinformation, J. Urol. 169 (2) (2003) 663–665.
[9] L.A. Baker, D. Sigman, R.I. Mathews, et al., An analysis of clinical outcomes using color Doppler testicular ultrasound for testicular torsion, Pediatrics 105 (3) (2000) 604–607.
[10] P. McLaren, A systematic review on the utility of ultrasonography in the diagnosis of testicular torsion in acute scrotum patients, Radiography 27 (3) (2021) 943–949.
[11] S. Ingram, A. Hollman, Colour Doppler sonography of the normal paediatric testis, Clin. Radiol. 49 (4) (1994) 266–267.
[12] Jr.G. Atkinson, L. Patrick, Jr.T. Ball, et al., .The normal and abnormal scrotum in children: evaluation with color Doppler sonography, AJR Am. J. Roentgenol. 158 (3) (1992) 613–617.
[13] A.N. Bandarkar, A.R. Blask, Testicular torsion with preserved flow: key sonographic features and value-added approach to diagnosis, Pediatr. Radiol. 48 (5) (2018) 735–744.
[14] P. Galina, V. Dermentzoglou, N. Baltogiannis, et al., Sonographic appearances of the epididymis in boys with acute testicular torsion but preserved testicular blood flow on color Doppler, Pediatr. Radiol. 45 (11) (2015) 1661–1671.
[15] M.M. Munden, J.L. Williams, W. Zhang, et al., Intermittent testicular torsion in the pediatric patient: sonographic indicators of a difficult diagnosis, Am. J. Roentgenol. 201 (4) (2013), 912-8.
[16] S. Cassar, S. Bhatt, H.J. Paltiel, et al., Role of spectral Doppler sonography in the evaluation of partial testicular torsion, J. Ultrasound Med. 27 (11) (2008) 1629–1638.
[17] V. Rafailidis, D.Y. Huang, G.T. Yusuf, et al., General principles and overview of vascular contrast-enhanced ultrasonography. Ultrasonography 39 (1) (2020) 22.
[18] M. Valentino, M. Bertolotto, L. Derchi, et al., Role of contrast enhanced ultrasound in acute scrotal diseases, Eur. Radiol. 21 (9) (2011) 1831–1840.
[19] D. Schreiber-Dietrich, X. Cui, F. Piscaglia, et al., Contrast enhanced ultrasound in pediatric patients: a real challenge, Z. für Gastroenterol. 52 (10) (2014) 1178–1184.
[20] P.S. Sidhu, V. Cantisani, A. Deganello, et al., Role of contrast-enhanced ultrasound (CEUS) in paediatric practice: an EFSUMB position statemen, Ultraschall der Medizin-Eur. J. Ultrasound 38 (01) (2017) 33–43.
[21] J. Yao, L.V. Wang, Photoacoustic tomography: fundamentals, advances and prospects, Contrast Media Mol. Imaging 6 (5) (2011) 332–345.
[22] P. Beard, Biomedical photoacoustic imaging, Interface Focus 1 (4) (2011) 602–631.
[23] L.V. Wang, J. Yao, A practical guide to photoacoustic tomography in the life sciences, Nat. Methods 13 (8) (2016) 627–638.
[24] A. Taruttis, V. Ntziachristos, Advances in real-time multispectral optoacoustic imaging and its applications, Nat. Photonics 9 (4) (2015) 219–227.
[25] A. Dima, V. Ntziachristos, Non-invasive carotid imaging using optoacoustic tomography, Opt. Express 20 (22) (2012) 25044–25057.
[26] Schulmeister K. , 2013. The upcoming new editions of IEC 60825–1 and ANSI Z136. 1–Examples on Impact for Classification and Exposure Limits. in International Laser Safety Conference. 2013. Laser Institute of America.
[27] Z. Li, H. Li, W. Xie, et al., In vivo determination of acute myocardial ischemia based on photoacoustic imaging with a focused transducer, J. Biomed. Opt. 16 (7) (2011), 076011.
[28] K. Okumura, J. Matsumoto, Y. Iwata, et al., Evaluation of renal oxygen saturation using photoacoustic imaging for the early prediction of chronic renal function in a model of ischemia-induced acute kidney injury, PLoS One 13 (12) (2018), e0206461.
[29] M. Chen, H.J. Knox, Y. Tang, et al., Simultaneous photoacoustic imaging of intravascular and tissue oxygenation, Opt. Lett. 44 (15) (2019) 3773–3776.
[30] J.R. Eisenbrey, M. Stanczak, F. Forsberg, et al., Photoacoustic oxygenation quantification in patients with Raynaud's: first-in-human results, Ultrasound Med. Biol. 44 (10) (2018) 2081–2088.
[31] A. Becker, M. Masthoff, J. Claussen, et al., Multispectral optoacoustic tomography of the human breast: characterisation of healthy tissue and malignant lesions using a hybrid ultrasound-optoacoustic approach, Eur. Radiol. 28 (2) (2018) 602–609.
[32] M. Masthoff, A. Helfen, J. Claussen, et al., Multispectral optoacoustic tomography of systemic sclerosis, J. Biophotonics 11 (11) (2018), e201800155.
[33] H. Thaker, C.P. Nelson, Adjuvant pharmacological and surgical therapy for testicular torsion: Current state of the art, J. Pediatr. Urol. 16 (6) (2020) 807–814.
[34] A. Raisi, A. Kheradmand, G. Farjanikish, et al., Nitroglycerin ameliorates sperm parameters, oxidative stress and testicular injury following by testicular torsion/detorsion in male rats, Exp. Mol. Pathol. 117 (2020), 104563.
[35] B.D. Coley, D.P. Frush, D.S. Babcock, et al., Acute testicular torsion: comparison of unenhanced and contrast-enhanced power Doppler US, color Doppler US, and radionuclide imaging, Radiology 199 (2) (1996) 441–446.
[36] J. Yang, G. Zhang, M. Wu, et al., Photoacoustic assessment of hemodynamic changes in foot vessels, J. Biophotonics 12 (6) (2019), e201900004.
[37] J. Yang, G. Zhang, W. Chang, et al., Photoacoustic imaging of hemodynamic changes in forearm skeletal muscle during cuff occlusion, Biomed. Opt. Express 11 (8) (2020) 4560–4570.
[38] T. Qiu, J. Yang, T. Pan, et al., Assessment of liver function reserve by photoacoustic tomography: a feasibility study, Biomed. Opt. Express 11 (7) (2020) 3985–3995.
[39] L. Huang, T.T. Li, H.B. Jiang, Thermoacoustic imaging of hemorrhagic stroke: a feasibility study with a human skull, Med. Phys. 44 (2017) 1494–1499.
[40] L. Yao, L. Xi, H. Jiang, Photoacoustic computed microscopy, Sci. Rep. 4 (2014) 4960.
[41] M.J. Cosentino, M. Nishida, R. Rabinowitz, et al., Histopathology of prepubertal rat testes subjected to various durations of spermatic cord torsion, J. Androl. 7 (1) (1986) 23–31.
[42] M.J. Cosentino, M. Nishida, R. Rabinowitz, et al., Histological changes occurring in the contralateral testes of prepubertal rats subjected to various durations of unilateral spermatic cord torsion, J. Urol. 133 (5) (1985) 906–911.
[43] M.A. Kroger-Jarvis, G.L. Gillespie, Presentation of testicular torsion in the emergency department, Adv. Emerg. Nurs. J. 38 (4) (2016) 295–299.
[44] V.J. Sharp, K. Kieran, A.M. Arlen, Testicular torsion: diagnosis, evaluation, and management, Am. Fam. Physician 88 (12) (2013) 835–840.
[45] P. Vaupel, A. Mayer, M. Höckel, Tumor hypoxia and malignant progression, Methods Enzymol. 381 (2004) 335–354.
[46] J. Xia, A. Danielli, Y. Liu, et al., Calibration-free quantification of absolute oxygen saturation based on the dynamics of photoacoustic signals, Opt. Lett. 38 (15) (2013) 2800–2803.
[47] J. Zötterman, M. Bergkvist, F. Iredahl, et al., Monitoring of partial and full venous outflow obstruction in a porcine flap model using laser speckle contrast imaging, J. Plast. Reconstr. Aesthetic Surg. 69 (7) (2016) 936–943.
[48] D. Rischin, R.J. Hicks, R. Fisher, et al., Prognostic significance of [18F]-misonidazole positron emission tomography–detected tumor hypoxia in patients with advanced head and neck cancer randomly assigned to chemoradiation with or without tirapazamine: a substudy of Trans-Tasman Radiation Oncology Group Study 98.02, J. Clin. Oncol. 24 (13) (2006) 2098–2104.
[49] R.B. Buxton, The physics of functional magnetic resonance imaging (fMRI), Rep. Prog. Phys. 76 (9) (2013), 096601.
[50] M. Ferrari, L. Mottola, V. Quaresima, Principles, techniques, and limitations of near infrared spectroscopy, Can. J. Appl. Physiol. 29 (4) (2004) 463–487.
[51] Y. Hoshi, Y. Yamada, Overview of diffuse optical tomography and its clinical applications, J. Biomed. Opt. 21 (9) (2016), 091312.
[52] X.D. Wang, X.Y. Xie, G.N. Ku, et al., Noninvasive imaging of hemoglobin concentration and oxygenation in the rat brain using high-resolution photoacoustic tomography, J. Biomed. Opt. 11 (2) (2006), 024015.
[53] Burgu B. AydogduO, P.U. Gocun, et al., Near infrared spectroscopy to diagnose experimental testicular torsion: comparison with Doppler ultrasound and immunohistochemical correlation of tissue oxygenation and viability, J. Urol. 187 (2) (2012) 744–750.
[54] G.A. Capraro, T.J. Mader, B.F. Coughlin, et al., Feasibility of using near-infrared spectroscopy to diagnose testicular torsion: an experimental study in sheep, Ann. Emerg. Med. 49 (4) (2007) 520–525.
[55] B. Hallacoglu, R. Matulewicz, H.J. Paltiel, et al., Noninvasive assessment of testicular torsion in rabbits using frequency-domain near-infrared spectroscopy: prospects for pediatric urology, J. Biomed. Opt. 14 (5) (2009), 054027.
[56] Shadgan B., Kajbafzadeh M., Nigro M., et al. Optical monitoring of testicular torsion using a miniaturized near infrared spectroscopy sensor. in Therapeutics and Diagnostics in Urology: Lasers, Robotics, Minimally Invasive, and Advanced Biomedical Devices. 2017. International Society for Optics and Photonics.
[57] C. García-Pastor, S. Benito-Martínez, V. Moreno-Manzano, et al., Mechanism and consequences of the impaired Hif-1α response to hypoxia in human proximal tubular HK-2 cells exposed to high glucose, Sci. Rep. 9 (1) (2019) 1–18.
[58] H. NakayamaA, Ide, A. Osaka, et al., The diagnostic accuracy of testicular torsion by doctors on duty using sonographic evaluation with color Doppler, Am. J. Men. 'S. Health 14 (5) (2020), 1557988320953003.
[59] H.G. Wright, H.J. Wright, Ultrasound use in suspected testicular torsion: an association with delay to theatre and increased intraoperative finding of non-viable testicle, N. Z. Med. J. 134 (1542) (2021) 50–55.
[60] I.A.S. Burud, S.M.I. Alsagoff, R. Ganesin, et al., Correlation of ultrasonography and surgical outcome in patients with testicular torsion, Pan Afr. Med. J. 36 (2020) 45.
[61] W.W. Lam, T.L. Yap, A.S. Jacobsen, Colour Doppler ultrasonography replacing surgical exploration for acute scrotum: myth or reality? Pedia Radio. 35 (6) (2005) 597–600.

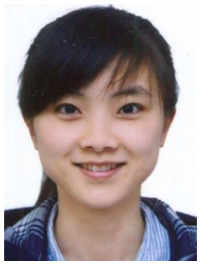

Qianru Yang is currently a doctor in Department of Ultrasound, West China Hospital, Sichuan University. She received his Ph.D. degree in 2020 from Sichuan University. She is now a post-doctoral fellowship at Sichuan University. Her research mainly focuses on the breast ultrasonography and the clinical application of photoacoustic imaging.

Lulu Yang is an attending physician in West China Hospital of Sichuan University. She got her Ph.D. in Clinical medicine from Sichuan University, China. She has worked in the field of clinical imaging, especially in ultrasonography.

Chihan Peng is currently a doctor in Department of Ultrasound, West China Hospital, Sichuan University. He received his Ph.D. degree in 2019 from Sichuan University. He completed his post-doctoral fellowship in 2022. His research mainly focuses on the liver ultrasonography and interventional ultrasound.

Xiaoxia Zhu is a research assistant of West China Hospital of Sichuan University of China. She received her Master's degree in 2012 from southwest University for nationalities of China with expertise in Veterinary Medicine.

Zhenru Wu is a Laboratory technician of West China Hospital, Sichuan University and Institute of Clinical Pathology at West China Hospital, Sichuan University. She received her master's degree in 2012 from Three Gorges University of China with expertise in ecology.

Lin Huang received the Ph.D. degree in optics from the University of Electronic Science and Technology, Chengdu, China, in 2015. He is currently an Associate Professor with the University of Electronic Science and Technology of China. His research is focused on discovering and developing fundamentally electromagnetic related imaging technologies for in vivo visualization of tissue at both the macroscopic and microscopic scales.

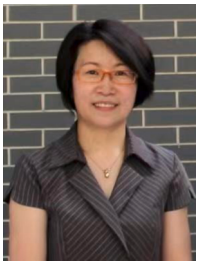

Yan Luo is currently the director and a Professor of Department of Ultrasound, West China Hospital, Sichuan University. She has been engaged in clinical and scientific research in ultrasound. Her current research interests include ultrasonography for abdominal diseases (especially liver diseases) and emerging imaging technologies.